Molecular Therapy
Oncolytics
Original Article

Promoting role of pentraxin-3 in esophageal squamous cell carcinoma

Zhirui Fan,[1,5] Yuanyuan Zheng,[2,3,5] Xiaoli Li,[2,5] Xiaoming Deng,[1] Yan Ba,[1] Kun Feng,[1] Jin Su,[1] Hui Wang,[1] Zhenhe Suo,[2,4] and Lifeng Li[2,3]

[1]Department of Chinese and Western Integrative Medicine, the First Affiliated Hospital of Zhengzhou University, Zhengzhou 450052, Henan, China; [2]Department of Oncology, the First Affiliated Hospital of Zhengzhou University, Zhengzhou 450052, Henan, China; [3]Internet Medical and System Applications of National Engineering Laboratory, the First Affiliated Hospital of Zhengzhou University, Zhengzhou 450052, Henan, China; [4]Department of Pathology, The Norwegian Radium Hospital, Oslo University Hospital, Institute of Clinical Medicine, University of Oslo, 999026 Montebello, Oslo, Norway

Pentraxin 3 (PTX3) is an inflammatory molecule that is closely related to the proliferation, invasion, and metastasis of cancer. In order to explore the role of PTX3 in the occurrence and development of esophageal carcinoma (ESCA), we modified the PTX3 gene in ESCA cell lines to obtain the model of gene knockout and overexpression and studied cell proliferation, cycle, apoptosis, migration ability, energy metabolism, and sensitivity to chemotherapy and radiotherapy. We observed the increase in cell proliferation, cycle, apoptosis, migration ability, and sensitivity to chemotherapy and radiotherapy in the PTX3 knockout model, while in the PTX3 overexpression model, these phenomena were significantly reduced. Knockout of the PTX3 also resulted in decreased cell glycolysis and increased oxidative phosphorylation, which is consistent with other findings that PTX3 affects the tumorigenic ability of cells and their sensitivity to docetaxel. In ESCA, SOX9 directly regulates the expression of PTX3, while human leukocyte antigen (HLA)-system-related genes are significantly upregulated when lacking PTX3. These results indicate that SOX9 may play a crucial role in regulating PTX3 and affecting the HLA system in ESCA.

INTRODUCTION

According to Global Cancer Statistics, the incidence and mortality of esophageal cancer (ESCA) ranked seventh and sixth, respectively.[1] The incidence and mortality of ESCA in China rank among top five in the world, and it is one of the main malignant tumors that threaten the health of Chinese residents. Esophageal squamous cell carcinoma (ESCC) is the primary histologic type of ESCA, with a high incidence observed in certain areas of China.[2] Early stage of ESCA is generally asymptomatic. Once symptoms appear, they have reached advanced stage, when surgery might not be possible, and can only be cured through comprehensive treatments, such as radiotherapy and chemotherapy. These are the reasons why the overall survival rate of ESCA patients remains low. Therefore, it is necessary to elucidate the underlying mechanisms of tumorigenesis in ESCC and to identify the new biomarkers to provide the therapeutic targets for improving diagnosis and treatment of ESCC.

Rudolf Virchow discovered the existence of inflammatory cells in tumor tissue a century ago and for the first time proposed the link between chronic inflammation and tumorigenesis.[3] Recurrent and persistent chronic inflammation may be the causative factor of tumorigenesis, as well as an important factor in promoting tumor and angiogenesis.[4,5]

Pentraxin 3 (PTX3) was discovered in 1992 as a member of the pentraxin family,[6] which plays an important role in tumor-associated inflammation in some published studies.[7] As one of the essential components of humoral innate immunity, PTX3 is a typical acute phase protein expressed by hematopoietic cells and stromal cells in response to primary pro-inflammatory stimuli and is involved in the innate immunity against pathogens, regulation of inflammation, and tissue remodeling.[8–10]

In this study, we first investigated the expression of PTX3 in human ESCC cells and then generated the PTX3 knockout and overexpression models in esophageal squamous carcinoma cell lines and discussed the mechanism of PTX3. Finally, we performed experiments on tumor formation in nude mice and drug sensitivity experiments to further confirm the previous results. This study explored the role of PTX3 gene in the development of ESCC and laid an experimental foundation for future in-depth study of targeted therapy for ESCC.

RESULTS

Generation of PTX3 gene knockout and PTX3 gene overexpression cell lines

To understand the expression of PTX3 in ESCC, we examined the expression of PTX3 gene and its expressed protein in normal

Received 15 June 2021; accepted 3 February 2022;
https://doi.org/10.1016/j.omto.2022.02.005.

[5]These authors contributed equally

Correspondence: Lifeng Li, PhD, Department of Oncology, the First Affiliated Hospital of Zhengzhou University, Zhengzhou 450052, Henan, China
E-mail: lilifeng0317@163.com
Correspondence: Zhenhe Suo, PhD, Department of Oncology, the First Affiliated Hospital of Zhengzhou University, Zhengzhou 450052, Henan, China
E-mail: zhenhes@medisin.uio.no

esophageal epithelial cells Het1A and three ESCC cell lines (KYSE140, EC109, and KYSE450). The results of quantitative real-time PCR (Figure 1A) and western blot (Figure 1B) showed that the expression of PTX3 in the three ESCC cell lines was higher than that in the esophageal epithelial cells Het1A. Among them, the expression of PTX3 in KYSE450 was the highest, which was selected as the target cell to generate a cell line stably transfected with PTX3.

PTX3 knockout cells were generated by CRISPR-Cas9 gene-editing technology. First, we designed three guide RNA (gRNA) sequences for the target sequence of PTX3 and connected the three gRNA sequences to the lentiviral backbone plasmid, respectively. The schematic diagram of the PTX3-gRNA-len recombinant plasmid was presented in Figure 1C. PCR analysis of the recombinant plasmid (Figure 1D) showed that the three gRNA base sequences were successfully ligated into the backbone plasmid. In order to screen for the most efficient PTX3-gRNA, these three recombinant plasmids were transfected into 293T cells, and their respective genomes were extracted. After the target sequence was amplified by PCR, the enzyme digestion treatment was carried out. As shown in Figure 1E, PTX3-gRNA3 was the most efficient by grayscale analysis, and it was used to package the virus and infect KYSE450 cells. After infection, the cells were screened with puromycin, and the selected cells were subjected to single cell culture. Finally, five monoclonal cells were obtained. The results of western blot (Figure 1F) showed that the three cell lines KO1, KO3, and KO4 successfully knocked out the PTX3 protein. Through gene editing type analysis (Figures 1G and 1H), it was found that both strands of genomic DNA of cell lines KO3 were mutated, and the number of bases of both strand mutations was 3n + 1 times, indicating that we successfully obtained PTX3 knockout cells with consistent genetic modification and stable inheritance (named KYSE450 PTX3$^{-/-}$). At the same time, we used lentiviral vector to construct a cell line that overexpressed the PTX3 gene stably. The three clones with the highest expression were shown in Figure 1I. In the subsequent experiments, we selected KYSE450 PTX3-5 cells with the highest expression of PTX3. The control cells were named KYSE450-NC, and the overexpression cells KYSE450 PTX3-5 were named KYSE450 PTX3-OV. Western blot (Figure 1J) revealed that PTX3 protein expression in KYSE450 PTX3-OV cells was significantly higher than KYSE450-NC.

PTX3 affected proliferation, cycle, apoptosis, and migration of KYSE450 cells

Cell proliferation was measured by Incucyte ZOOM, and the results showed that the growth rate of KYSE450 PTX3$^{-/-}$ cells was significantly slower than that of KYSE450 cells ($p < 0.001$; Figure 2A). In addition, KYSE450 PTX3-OV cells grew significantly faster than KYSE450-NC cells, with the greatest difference at 24 h ($p < 0.001$; Figure 2B). For further analysis, cell cycle and cell apoptosis were detected by flow cytometry. Cell cycle assay (Figure 2C) showed that, after knockout of PTX3 gene, the proportion of cells in the dividing phase decreased, and the cells were blocked in G0/G1 phase. The proportion of G0/G1 phase cells of KYSE450 PTX3$^{-/-}$ cells was significant increased ($p < 0.001$), while the proportion of cells in S phase ($p < 0.001$) and G2/M phase ($p < 0.05$) decreased. Apoptosis results (Figure 2D) showed that the early apoptosis (propidium iodide [PI](+) Annexin V [AV](−)) of KYSE450 PTX3$^{-/-}$ was significantly increased, indicating that knocking out PTX3 can induce apoptosis. In contrast, after the overexpression of PTX3 gene, the proportion of cells in the dividing phase increased, the proportion of cells in the G0/G1 phase of KYSE450 PTX3-OV cells decreased, and the proportion of cells in the S phase cells increased significantly ($p < 0.05$; Figure 2E). In Figure 2F, the early apoptosis (PI(+)AV(−)) of KYSE450 PTX3-OV cells was significantly lower than that of KYSE450-NC, and the difference was statistically significant ($p < 0.05$), suggesting that overexpression of PTX3 can induce a decrease in apoptosis. All the results indicated that PTX3 knockout arrest cells in G0/G1 phase inhibited cell proliferation and promoted apoptosis, but overexpression of PTX3 accelerated the cell cycle, decreased cell apoptosis, and promoted cell proliferation.

To understand the effect of PTX3 on cell migration, we performed wound-healing test and transwell migration experiments. The results (Figures 2G and 2H) showed that the healing rate of KYSE450 PTX3$^{-/-}$ was significantly slower than that of KYSE450 cells, and the transmembrane ability was significantly lower than that of KYSE450 cells. On the contrary, the healing rate of KYSE450 PTX3-OV cells was faster than that of KYSE450-NC cells, and the transmembrane ability of KYSE450 PTX3-OV cells was much higher (Figures 2I and 2J).

PTX3 affected the sensitivity of KYSE450 cells to chemotherapy and radiotherapy

To test whether the PTX3 gene affects the sensitivity of KYSE450 cells to chemotherapeutic drugs, we co-cultured docetaxel and cisplatin with cells. Growth curve results by Incucyte Zoom (Figures 3A and 3C) showed that the proliferative capacity of cells treated with chemotherapeutic drugs was reduced, while KYSE450 PTX3$^{-/-}$ cells were more susceptible to chemotherapy than KYSE450. The results of plate cloning experiments were consistent with the above results. When the concentrations of docetaxel (Figure 3B) and cisplatin (Figure 3D) were raised, the number of cell clones decreased, and the number of clones of KYSE450 PTX3$^{-/-}$ cells was smaller than that of the corresponding KYSE450 group ($p < 0.05$). The above results indicated that knockout of the PTX3 gene results in increased chemosensitivity of KYSE450 cells. However, the overexpression of PTX3 gene resulted in decreased chemosensitivity of KYSE450 cells. From the growth curve, KYSE450-NC cells were more susceptible to chemotherapy than KYSE450 PTX3-OV (Figures 3E and 3G). Exposure to increasing concentration of docetaxel (Figure 3F) and cisplatin (Figure 3H) resulted in decreased number of clone formation, but the clone number of KYSE450 PTX3-OV cells was larger than that of the corresponding KYSE450-NC group ($p < 0.01$).

To assess the effect of PTX3 on the sensitivity of cell radiotherapy, we performed the plate clone formation assay. As shown in Figure 3I, after treatment with 0 Gy, 2 Gy, 4 Gy, 6 Gy, and 8 Gy dose of radiotherapy, the number of KYSE450 PTX3$^{-/-}$ cell clones was

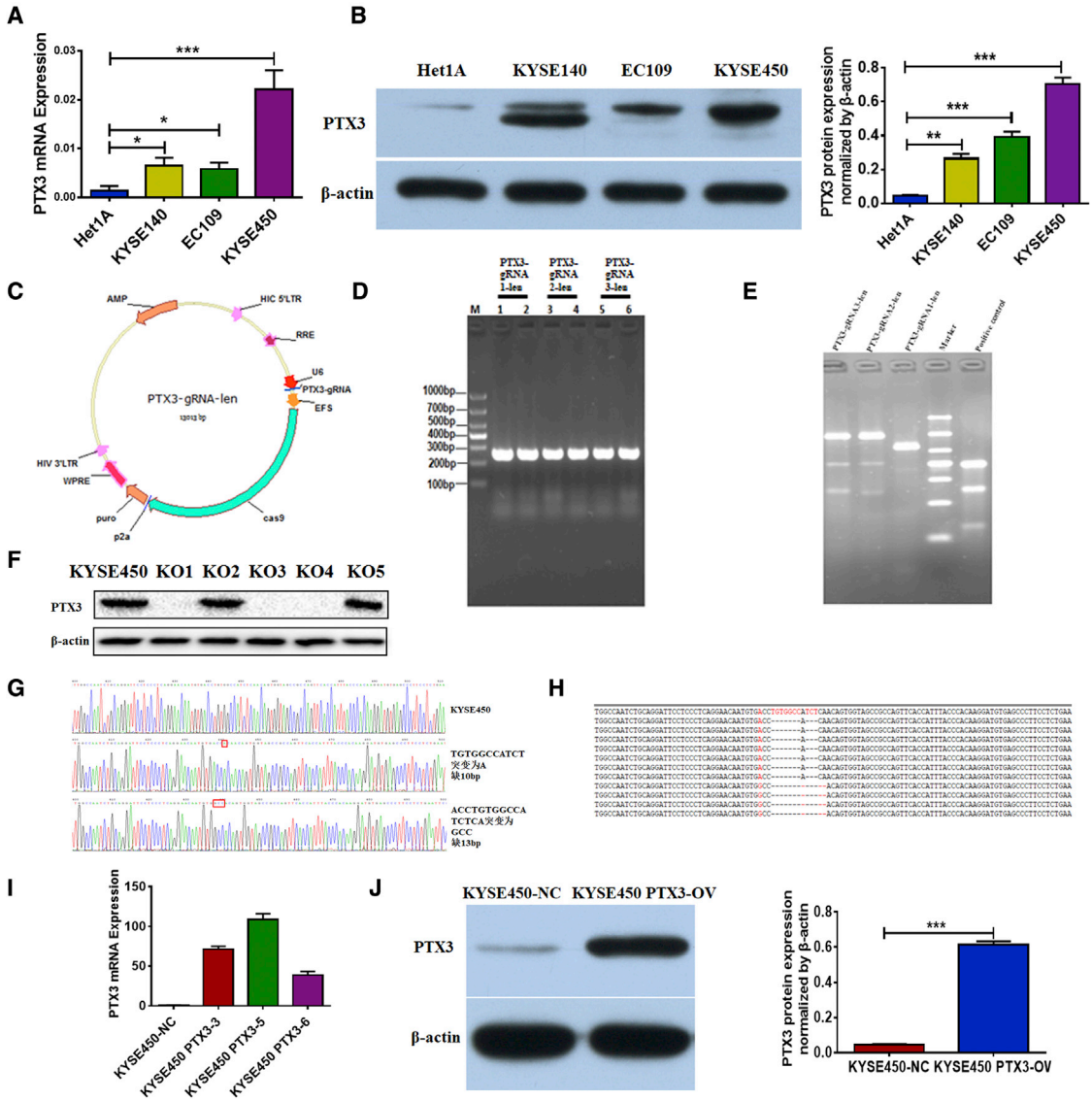

Figure 1. Expression of PTX3 in normal esophageal epithelium and esophageal cancer cells

(A) Gene expression of PTX3 in esophageal epithelial cells and ESCC detected by RT-PCR. (B) Protein expression of PTX3 in esophageal epithelial cells and ESCC detected by western blot are shown. (C) PTX3-gRNA-len plasmid map is shown. (D) PCR identification result of PTX3-gRNA-len recombinant plasmid bacterial solution is shown (M, marker; 1 and 2 represent PTX3-gRNA1-len, 3 and 4 represent PTX3-gRNA2-len, and 5 and 6 represent PTX3-gRNA3-len). (E) T7E1 mismatch enzyme detects the knockout efficiency of each recombinant plasmid. The bands of marker from top to bottom are 1,000 bp, 700 bp, 500 bp, 400 bp, 300 bp, 200 bp, and 100 bp. (F) The PTX3 protein knockout of cultured monoclonal cells is identified by western blot. (G) Analysis of PTX3-gRNA-mediated gene-editing types is shown. Analysis of the sequencing results of TA clones of monoclonal cells is shown, and the red box indicates the base after mutation. (H) The single-strand DNA sequences of KYSE450 and TA cloning two sequencing results are shown. (I) PTX3 gene expression in the control cells and the three clones with the highest PTX3 expression is shown. (J) PTX3 protein expression in the control group and PTX3 overexpression group is shown. *$p < 0.05$, **$p < 0.01$, and ***$p < 0.001$.

significantly decreased compared with the corresponding KYSE450 cells ($p < 0.05$), suggesting that knockout of PTX3 can increase the sensitivity of cell radiotherapy. On the other hand, after 0 Gy, 2 Gy, 4 Gy, 6 Gy, and 8 Gy radiotherapy, KYSE450 PTX3-OV cell clone number was significantly increased compared with the corresponding KYSE450-NC cells ($p < 0.05$; Figure 3J), suggesting that the overexpression of PTX3 gene cells resulted in resistance to radiotherapy.

PTX3 affected energy metabolism of KYSE450 cells

To reveal the effect of PTX3 on energy metabolism of KYSE450 cells, we examined the oxygen consumption rate (OCR) and extracellular acidification rate (ECAR) of the cells by using a Seahorse XFe96 Extracellular Flux Analyzer. The basic value of ECAR reflects the non-glycolysis acid production value of the cells. After adding glucose, it represents the glycolysis ability of the cells at

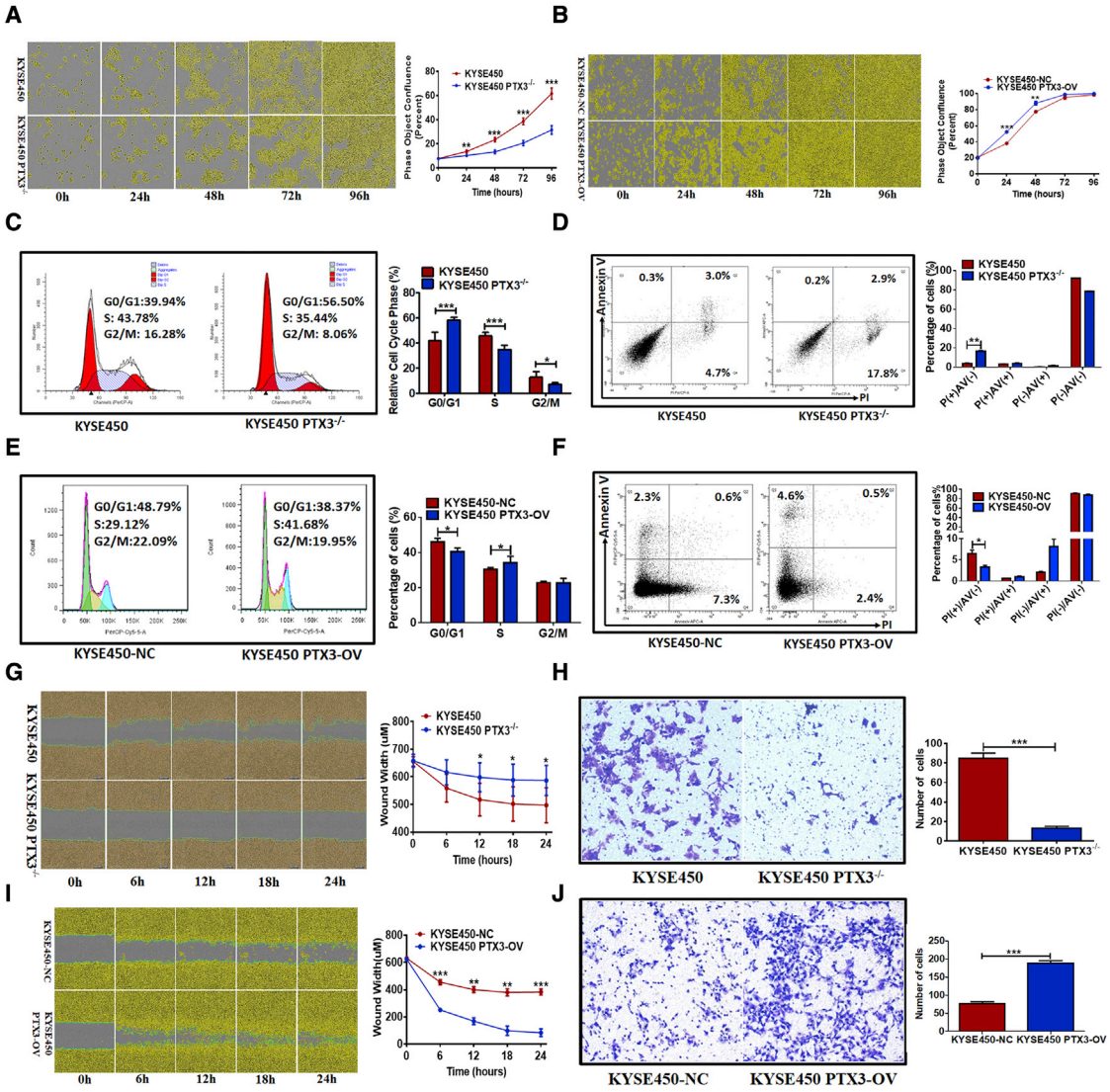

Figure 2. The effect of PTX3 on esophageal cancer cells

(A) Growth of KYSE450 and KYSE450 PTX3$^{-/-}$ cells and the cell growth curve measured by Incucyte ZOOM. (B) Growth of KYSE450 and KYSE450 PTX3-OV cells and the cell growth curve detected through Incucyte ZOOM are shown. (C) Effect of PTX3 knockout on the cell cycle by flow cytometry is shown. (D) Effects of PTX3 knockout on cell apoptosis analyzed by flow cytometry are shown. (E) Effects of PTX3 overexpression on cell cycle analyzed by flow cytometry are shown. (F) Effects of PTX3 overexpression on cell apoptosis analyzed by flow cytometry are shown. (G) Effects of PTX3 knockout on cell migration ability assessed by scratch test are shown. (H) Effect of PTX3 knockout on cell migration is measured by the transwell migration assay. (I) Effects of PTX3 overexpression on cell migration measured by scratch test are shown. (J) Effect of PTX3 overexpression on cell migration is measured by transwell migration assay. *p < 0.05, **p < 0.01, and ***p < 0.001.

this time. Upon addition of oligomycin, it reflects the maximum glycolysis capacity of the cells, and the increased value represents the glycolysis potential of the cell. The results showed that the basic glycolysis ability of KYSE450 PTX3$^{-/-}$ cells (12.01 ± 8.2 mpH/min) was lower than that of KYSE450 cell glycolysis (24.73 ± 7.16 mpH/min; $p < 0.05$); KYSE450 PTX3$^{-/-}$ cells had less glycolytic acid production reserve than KYSE450 cells (Figure 4A; $p < 0.01$), which indicated that KYSE450 PTX3$^{-/-}$ has worse glycolysis ability than KYSE450. OCR was performed under basal and stressed conditions in the presence of oligomycin, phenylhydrazone (carbonyl cyanide-p-trifluoromethoxyphenylhydrazone [FCCP]), and rotenone and antimycin A. The OCR results showed that the basal oxygen consumption of KYSE450 PTX3$^{-/-}$ cells was 173.37 ± 36.10 pmol/min, which was significantly higher than that of KYSE450 cells (139.02 ± 13.49 pmol/min; $p = 0.005$; Figure 4B). The uncoupler FCCP can stimulate the increase of cellular oxygen consumption, and the difference between the increase in oxygen consumption and basic oxygen consumption after stimulation reflects the respiratory reserve capacity of the cell mitochondrial. After adding FCCP, the oxygen consumption of

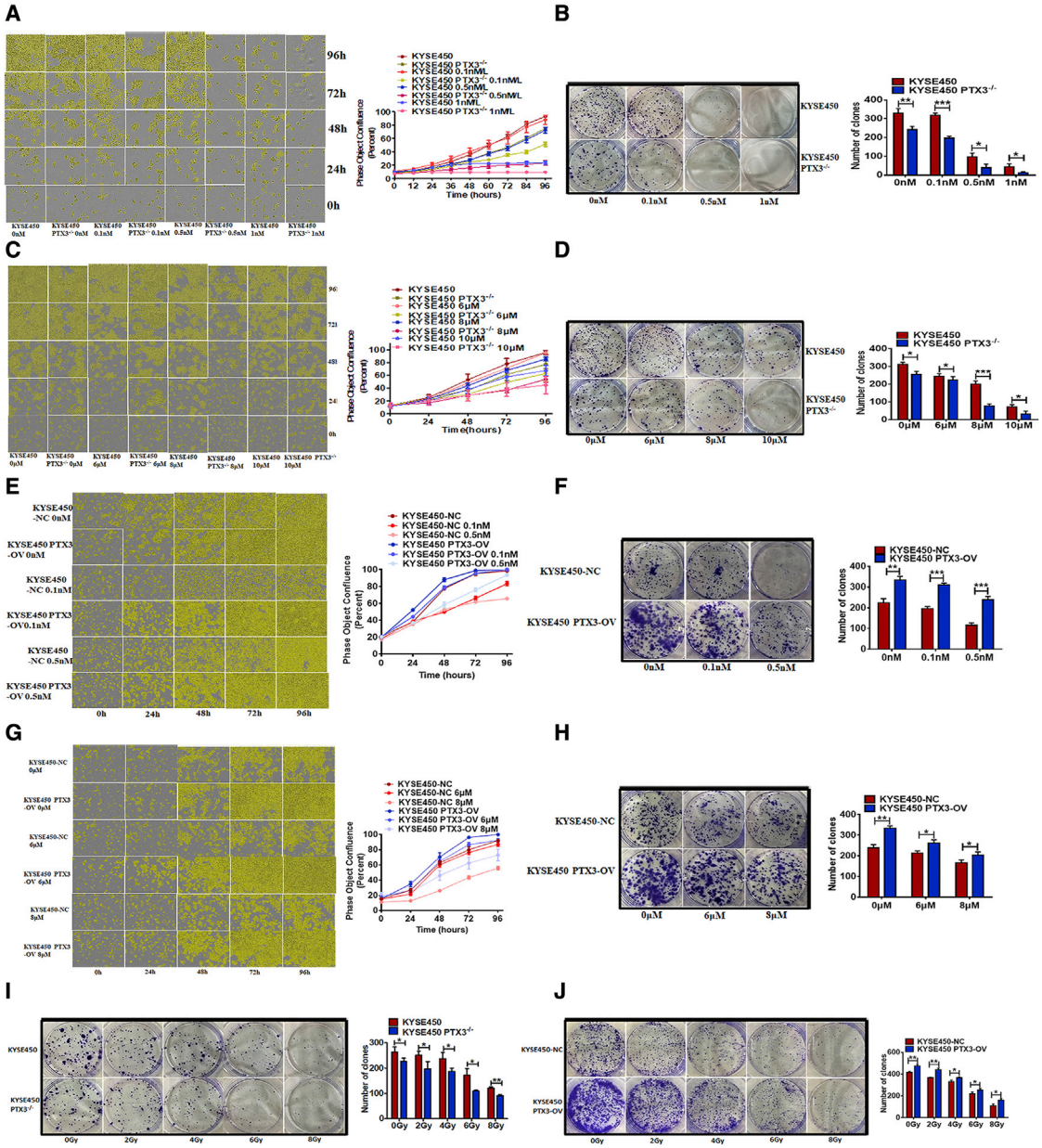

Figure 3. PTX3 affected the sensitivity of KYSE450 cells to chemotherapy and radiotherapy

(A) The difference in proliferation of KYSE450 and KYSE450 PTX3$^{-/-}$ cells treated with different concentrations of docetaxel (0 nM, 0.1 nM, 0.5 nM, and 1 nM) determined by Incucyte ZOOM. (B) Effects of different concentrations of docetaxel (0 nM, 0.1 nM, 0.5 nM, and 1 nM) on clone formation ability of KYSE450 and KYSE450 PTX3$^{-/-}$ cells detected by clone formation experiment are shown. (C) The Incucyte ZOOM was used to determine the difference in proliferation of KYSE450 and KYSE450 PTX3$^{-/-}$ cells treated with different concentrations of cisplatin (0 μM, 6 μM, 8 μM, and 10 μM) chemotherapy. (D) Clone formation experiment was used to detect the effect of different concentrations of cisplatin (0 μM, 6 μM, 8 μM, and 10 μM) chemotherapy on cloning ability of KYSE450 and KYSE450 PTX3$^{-/-}$ cells. (E) Difference in proliferation of KYSE450-NC and KYSE450 PTX3-OV cells treated with different concentrations of docetaxel (0 nM, 0.1 nM, and 0.5 nM) chemotherapy detected by Incucyte ZOOM is shown. (F) Effect of different concentrations of docetaxel (0 nM, 0.1 nM, and 0.5 nM) chemotherapy on the cloning ability of KYSE450-NC and KYSE450 PTX3-OV cells tested by clone formation experiment is shown. (G) Incucyte ZOOM was used to determine the difference in proliferation of KYSE450-NC and KYSE450 PTX3-OV cells treated with different concentrations of cisplatin (0 μM, 6 μM, and 8 μM) chemotherapy. (H) Clone formation experiment to detect the effects of different concentrations of cisplatin (0 μM, 6 μM, and 8 μM) chemotherapy on the cloning ability of KYSE450-NC and KYSE450 PTX3-OV cells is shown. (I) The effect of PTX3 knockout on the sensitivity of cell radiotherapy is shown. (J) Effect of PTX3 overexpression on the sensitivity of cell radiotherapy is shown. *$p < 0.05$, **$p < 0.01$, and ***$p < 0.001$.

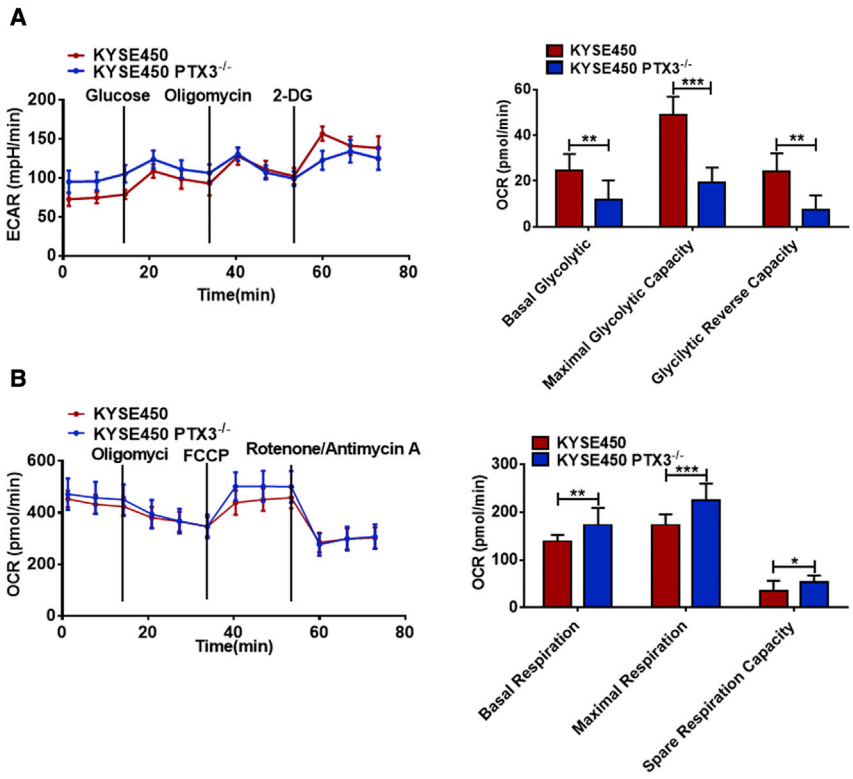

Figure 4. The cell energy metabolism meter detects the OCR and ECAR of the cells

(A) Line chart of cellular acidification rate and corresponding histogram of cell acid discharge rate. (B) The basic OCR in KYSE450 and KYSE450 PTX3$^{-/-}$ cells and corresponding histogram are shown.

KYSE450 PTX3$^{-/-}$ cells increased to 225.77 ± 34.08 pmol/min, while the respiration rate of KYSE450 cells increased only slightly (139.02 ± 13.49 pmol/min), and the respiratory reserve capacity of KYSE450 PTX3$^{-/-}$ cells was significantly higher than that of KYSE450 cells, indicating that KYSE450 PTX3$^{-/-}$ cells have better oxidative phosphorylation ability than KYSE450. The above results demonstrated that, after PTX3 was knocked out, the cell glycolysis ability was weakened, while the phosphorylation capacity tended to be enhanced.

PTX3 can be used as an indicator of the malignant degree of ESCC

To investigate the expression of PTX3 in ESCC, we conducted an immunohistochemical study. The results showed that, in ESCC tissue samples, PTX3 protein staining was cytoplasmic staining, and the expression of PTX3 was negative in normal esophageal tissues (Figure 5A). The relationship between the expression of PTX3 protein and the clinicopathological parameters of 294 patients with ESCC was shown in Table 1. The expression of PTX3 protein was negatively correlated with survival ($p = 0.000$) and positively correlated with tumor, node, and metastasis (TNM) stage ($p = 0.020$) and clinical stage ($p = 0.003$). PTX3 protein was positively expressed in 123/155 (79.35%) patients who died within 1 year, and among the patients whose survival time was greater than 5 years, the positive expression of PTX3 protein was 74/139 (53.24%). In the tumor tissues of pT3-pT4 patients, the positive expression of PTX3 protein was 133/191 (69.63%). The positive expression of PTX3 protein in the clinical stage III to IV patients was 143/201 (71.14%; Table 1).

Kaplan-Meier and log rank tests were used to calculate and compare survival, and the relationship between PTX3 protein expression and survival in 294 patients with ESCC was assessed. The data showed that the overall survival rate of 294 patients with ESCC was 36.05%, and the median follow-up time was 50 months. Among them, 188 patients died during the follow-up period. In all patients, 9 (3.06%) PTX3-negative cases, 88 (29.93%) PTX3 weak-positive cases, and 197 cases (67.01%) PTX3-positive cases were observed. Statistical analysis of Kaplan-Meier survival curves showed that expression of PTX3 was significantly associated with shorter survival of patients with ESCC, and it was a risk factor for shorter survival of patients with ESCC ($p < 0.001$; Figure 5B).

According to the above-mentioned clinicopathological parameters and the expression of PTX3 in tumor cells, the Cox proportional hazards regression method was used for univariate and multivariate analysis. Our findings suggested that PTX3 expression (hazard ratio [HR] = 2.484; 95% confidence interval [CI]: 1.665–3.708; $p = 0.000$), age (HR = 0.482; 95% CI: 0.333–0.696; $p = 0.000$), tumor size (HR = 1.287; 95% CI: 1.018–1.627; $p = 0.035$), TNM stage (HR = 1.951; 95% CI: 1.173–3.245; $p = 0.010$), and lymph node metastasis (HR = 2.094; 95% CI: 1.507–2.910; $p = 0.000$) were independent prognostic factors for patients with ESCC (Table 2).

SOX9 regulated PTX3, affected HLA system, and promoted tumor progression

To clarify the upstream mechanism of PTX3 in ESCC, we used NCBI to search the promoter DNA sequence of PTX3 (https://www.ncbi.nlm.nih.gov/pubmed). Then, we used the JASPAR database (http://jaspar.binf.ku.dk/) and QIAGEN (http://www.sabiosciences.com/chipqpcrsearch.php?app=TFBS) to predict that SOX9 might be the upstream transcription factor of PTX3. To further elucidate the mechanism of SOX9 regulating the expression of PTX3 in ESCC, we used the PROMO website and JASPAR website to analyze the 5′-terminal regulatory region of PTX3, predict the SOX9 binding sequence, and select the highest scoring sequence (5′-TCATTGTTC-3′) for correlation verification (Figure 6A). To

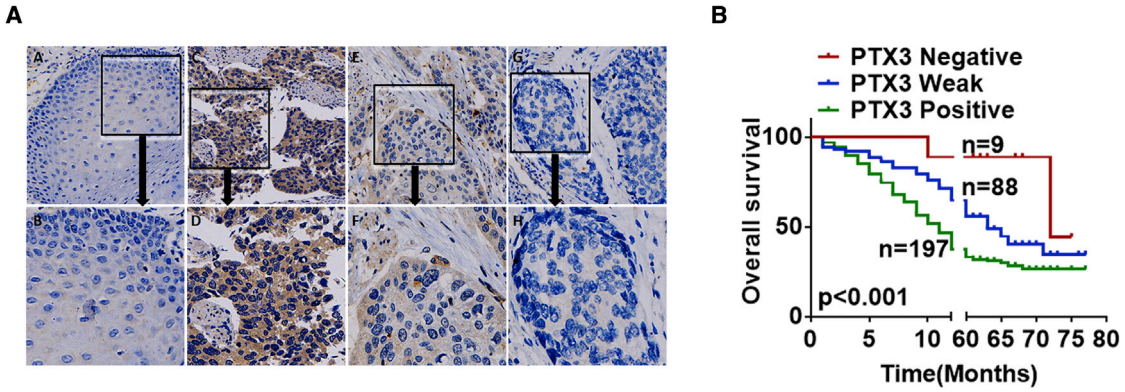

Figure 5. Expression of PTX3 protein in normal tissues and cancer tissues of the esophagus

(A) Negative expression of PTX3 protein in esophageal tissue (A, 200×; B, 400×); C and D show positive expression of PTX3 protein in ESCC tissue (C, 200×; D, 400×); E and F show weakly positive expression of PTX3 protein in ESCC tissue (E, 200×; F, 400×); and G and H show negative expression of PTX3 protein in ESCC tissue. The black arrow indicates the position of the 400× picture in the 200× picture. (B) The correlation between the expression of PTX3 protein and the prognosis of patients with ESCC is shown. Kaplan-Meier survival curve shows that PTX3 protein expression is positively correlated with poor prognosis of patients with ESCC.

determine whether SOX9 directly regulates transcription of the PTX3 gene, we performed a chromatin immunoprecipitation (ChIP) experiment. The results of DNA agarose gel electrophoresis after sonication and protein-DNA decrosslinking showed that the DNA fragments were mainly concentrated between 200 and 700 bp (Figure 6B). The electrophoresis of the PCR product was shown in Figure 7B. The amplified band from the input DNA without antibody precipitation was the brightest, and the DNA precipitated by the positive antibody as template amplified the target band. However, the DNA electrophoresis obtained by precipitation of the immunoglobulin G (IgG) antibody was substantially band free and showed little amplification products. The above results demonstrated that the transcription factor SOX9 binds to the promoter of PTX3.

To verify whether SOX9 regulates PTX3 *in vitro* level, we performed an electrophoretic mobility shift assay (EMSA) experiment. The results (Figure 6C) showed that there was no specific binding band in the reaction without protein addition, but when the probe bound to the protein, a specific protein-probe complex band appeared above the lane, indicating that the PTX3 protein bound to the SOX9 probe. To verify the specificity of the binding, a 200-fold unlabeled probe was added to the labeled probe to compete for binding. As a result, the band of the probe-binding protein completely disappeared. In the mutation competition, the binding site of SOX9 was mutated, and the PTX3 protein could not bind to the mutant probe.

To further verify the regulation of SOX9 on PTX3, we used small interfering RNA (siRNA) for transfection, and quantitative real-time PCR to detect the transfection efficiency of SOX9 after 48 h of transfection. Our findings suggested that the expression of SOX9 gene in SOX9 Si1 and SOX9 Si2 cells was significantly lower than that of the control group ($p < 0.05$), and the expression of PTX3 gene and protein after SOX9 silencing was significantly lower than that of the control groups ($p < 0.05$). It is suggested that the expression of SOX9 affects the expression of PTX3, and SOX9 can regulate the transcriptional expression of PTX3 (Figure 6D). Furthermore, in order to observe the changes in the biological function of cells after SOX9 silencing, we evaluated and tested the cell proliferation, cycle, and apoptosis. The consequence of plate cloning experiments showed (Figure 6E) that, after SOX9 was silenced, the cell proliferation rate was significantly reduced ($p < 0.001$). The results of cell cycle were shown as Figure 6F. After transient transfection of SOX9, the proportion of G0/G1 phase cells in KYSE450 cells increased significantly ($p < 0.05$), and the proportion of both S phase and G2/M phase cells decreased. The identification of cell cycle showed that, after SOX9 was silenced, the proportion of actively dividing cells decreased, and most cells were blocked in G0/G1 phase. Flow cytometry detection of apoptosis showed (Figure 6G) that, after SOX9 silencing, both early apoptosis (PI(+)AV(−)) and late apoptosis (PI(+)AV(+)) increased, and the difference was statistically significant ($p < 0.05$). The results suggested that SOX9 silencing slowed down cell proliferation, induced cell-cycle arrest, and induced apoptosis.

In order to understand the co-expression of SOX9 and PTX3, we examined the SOX9 protein expression in ESCC tissue samples. SOX9 staining was mainly nuclear staining (Figure 6H). Correlation analysis of SOX9 and PTX3 protein expression in the same patients' tissues showed that the tissues with high SOX9 expression also had high PTX3 expression. Likewise, tissues that expressed lower level of SOX9 also had lower expression of PTX3 (Figure 6I). This indicated that PTX3 protein expression was high in the SOX9 high expression region and vice versa. At the same time, a positive correlation between the co-localized expression of SOX9 and PTX3 in ESCC samples was determined by immunofluorescence detection (Figure 6J). All these results indicated that there is a positive correlation between the expression of SOX9 and PTX3 in ESCC.

In order to explore the molecular mechanism of changes in KYSE450 cells after knocking out the PTX3 gene, we performed

Table 1. The associations of PTX3 expression levels and the clinicopathological characteristics in ESCC

	PTX3 expression				
Clinicopathological variable	n	Positive	Weak positive	Negative	p value[a]
Survival					
≤1 year	155	123 (79.35%)	31 (20.00%)	1 (0.65%)	0.000
≥5 years	139	74 (53.24%)	57 (41.01%)	8 (5.76%)	
Age (years)					
≤60	134	93 (69.40%)	38 (28.36%)	3 (2.24%)	0.619
>60	160	104 (65.00%)	50 (31.25%)	6 (3.75%)	
Gender					
Male	175	117 (66.86%)	54 (30.86%)	4 (2.29%)	0.614
Female	119	80 (67.23%)	34 (28.57%)	5 (4.20%)	
Tumor size (mm)					
<30	162	103 (63.58%)	51 (31.48%)	8 (4.94%)	0.236
30–60	88	61 (69.32%)	26 (29.55%)	1 (1.14%)	
>60	44	33 (75.00%)	11 (25.00%)	0 (0.00%)	
Tumor location					
Upper	54	37 (68.52%)	17 (31.48%)	0 (0.00%)	0.215
Middle	199	137 (68.84%)	56 (28.14%)	6 (3.02%)	
Lower	41	23 (56.10%)	15 (36.59%)	3 (7.32%)	
Histologic grade					
Well	11	7 (63.64%)	4 (36.36%)	0 (0.00%)	0.804
Moderate	211	140 (66.35%)	63 (29.86%)	8 (3.79%)	
Poor	72	50 (69.44%)	21 (29.17%)	1 (1.39%)	
TNM stage					
pT1-pT2	103	64 (62.14%)	32 (31.07%)	7 (6.80%)	0.020
pT3-pT4	191	133 (69.63%)	56 (29.32%)	2 (1.05%)	
Clinical stage					
I-II	93	54 (58.06%)	32 (34.41%)	7 (7.53%)	0.003
III-IV	201	143 (71.14%)	56 (27.86%)	2 (1.00%)	
Lymph node metastasis					
No	174	115 (66.09%)	53 (30.46%)	6 (3.45%)	0.860
Yes	120	82 (68.33%)	35 (29.17%)	3 (2.50%)	
Distant metastasis					
No	292	197 (64.47%)	86 (29.45%)	9 (3.08%)	0.095
Yes	2	0 (0.00%)	2 (100.00%)	0 (0.00%)	

[a]Chi-square test

high-throughput transcriptome sequencing on a total of six samples of KYSE450 and KYSE450 PTX3$^{-/-}$ cells. After analysis, the expression of multiple differentially expressed genes (DEGs) was either significantly up-regulated or down-regulated, including 4,292 up-regulated genes and 4,085 down-regulated genes (Figure 1A). Once analyzing all the differential genes had been done, the differential gene expression heatmap that showed the expression of the differential genes was then obtained (Figure 1B). Based on the detected differential genes, Gene Ontology (GO) functional enrichment analysis and Kyoto Gene and Genome Encyclopedia (KEGG) biological pathway enrichment analysis were performed. GO functional analysis includes three aspects: biological process (BP), cellular component (CC), and molecular function (MF). The top three groups observed with the greatest differences in BP are cellular process, single-organism process, and metabolic process. The CC part had the greatest correlation with cell, cell part, and organelle. Finally, in the MF classification, the difference between participating in binding, catalytic activity, and molecular function

Table 2. Univariate and multivariate survival analysis of ESCC patients using Cox relative risk

	Univariate analysis		Multivariate analysis	
Variable	HR (95% CI)	p value	HR (95% CI)	p value
PTX3 expression in tumor	2.349 (1.590–3.468)	0.000	2.484 (1.665–3.708)	0.000
Age (no more than 60 versus >60)	0.591 (0.411–0.850)	0.005	0.482 (0.333–0.696)	0.000
Sex (male , female)	1.077 (0.919–1.262)	0.361	1.134 (0.964–1.334)	0.128
Tumor size (<30, 30–60, >60)	0.536 (0.350–0.822)	0.004	1.287 (1.018–1.627)	0.035
TNM stage (T1-T2 versus T3-T4)	2.727 (1.829–4.065)	0.000	1.951 (1.173–3.245)	0.010
Clinical stage (I-IIversus III-IV)	2.287 (1.534–3.408)	0.000	1.064 (0.635–1.784)	0.813
Lymph node metastasis (no versus yes)	2.419 (1.757–3.332)	0.000	2.094 (1.507–2.910)	0.000
Distant metastasis (no versus yes)	0.961 (0.134–6.866)	0.968	0.304 (0.041–2.276)	0.247

HR, hazard ratio; 95% CI, 95% confidence interval.

regulator was the largest (Figure 1C). The results of KEGG pathway classification were shown in Figure 1D, and the enrichment results were shown in Figure 1E. Endocytosis, focal adhesion, and herpes simplex infection-signaling pathways had the most genes enriched. Through differential gene analysis, we found that a series of genes (HLA-A, HLA-B, HLA-C, HLA-DMA, HLA-DMB, HLA-DOA, HLA-DPA1, HLA-DQB2, HLA-DRA, HLA-DRB1, HLA-DRB5, HLA-DQA1, HLA-DQB1, and CD74) related to the HLA system in KYSE450 cells, which were significantly up-regulated after PTX3 knockout (Figure 6K), and these genes were concentrated in the herpes simplex infection pathway (Figure 6L). We verified the expression of these genes in the cells by RT-PCR. The results (Figure 6M) showed that the expression of these genes in the KYSE450 PTX3$^{-/-}$ group was significantly up-regulated, which was consistent with the transcriptome sequencing results. At the same time, we selected HLA class I ABC, HLA DR + DP + DQ, and CD74 antibodies for verification in 101 ESCC cases (Figure 6N), of which 57 patients died within 1 year and 44 patients survived for more than 5 years. The results (Table 3) suggested that the expression of HLA class I ABC, HLA DR + DP + DQ, and CD74 was significantly correlated with the survival rate of ESCC patients ($p < 0.05$), and the expression of the survival rate over 5 years was higher, which were 67.57%, 73.33%, and 57.14%, respectively. Kaplan-Meier survival curve and log rank test proved that the expression of HLA class I ABC, HLA DR + DP + DQ, and CD74 in ESCC was significantly correlated with longer survival time (Figure 6N; $p < 0.05$).

PTX3 affected the tumorigenicity of KYSE450 cells

In order to explore the effect and mechanism of PTX3 on tumorigenicity *in vivo*, we used PTX3 knockout and overexpression cells model (5×10^6 cells/each mice) to inoculate subcutaneously in nude mice. After the tumor volume reached about 80 mm^3, the administration group began to receive 7 mg/kg docetaxel intraperitoneally (twice a week). In the meantime, the non-administration group was intraperitoneally injected with solvent control (twice a week). The body weight and tumor data were monitored, and the animals were sacrificed 4 weeks after inoculation.

Subcutaneous tumors appeared in 24 nude mice about 1 week after inoculation, and the tumor formation rate was 100% (Figure 7A). The tumor growth rate of the KYSE450 PTX3$^{-/-}$ group was significantly slower than that of KYSE450 group, and the KYSE450 PTX3$^{-/-}$ cells were more sensitive to docetaxel (Figures 7B and 7C). The weight of the four groups of nude mice increased gradually. At the time of sacrifice, the average weights of the four groups were 22.525 ± 1.309 g (KYSE450 group), 21.927 ± 1.034 g (KYSE450 administration group), 22.755 ± 1.185 g (KYSE450 PTX3$^{-/-}$ group), and 21.910 ± 1.337 g (KYSE450 PTX3$^{-/-}$ administration group). The difference was not statistically significant (Figure 7D; $p > 0.05$). The average tumor weights at the time of execution were 0.793 ± 0.276 g (KYSE450 group), 0.300 ± 0.154 g (KYSE450 administration group), 0.462 ± 0.270 g (KYSE450 PTX3$^{-/-}$ group), and 0.062 ± 0.036 g (KYSE450 PTX3$^{-/-}$ administration group). The difference was statistically significant (Figure 7E; $p < 0.05$). The tumor growth inhibition rate was 62.17% in the KYSE450 group and 86.58% in the KYSE450 PTX3$^{-/-}$ group.

However, the tumor growth rate of the KYSE450 PTX3-OV group was significantly faster than that of the KYSE450-NC group, and it was not sensitive to docetaxel (Figures 7F–7H). The average body weights of the four groups at the time of execution were 24.458 ± 0.649 g (KYSE450-NC group), 23.797 ± 1.434 g (KYSE450-NC administration group), 24.440 ± 1.283 g (KYSE450 PTX3-OV group), and 21.812 ± 1.778 g (KYSE450 PTX3-OV administration group). The difference was not statistically significant (Figure 7I; $p > 0.05$). The average tumor weights at the time of execution were 0.640 ± 0.187 g (KYSE450-NC group), 0.303 ± 0.143 g (KYSE450-NC administration group), 0.848 ± 0.084 g (KYSE450 PTX3-OV group), and 0.622 ± 0.292 g (KYSE450 PTX3-OV administration group). The difference was statistically significant (Figure 7J; $p < 0.05$). The tumor growth inhibition rate was 52.66% in the KYSE450-NC group but only 26.65% in the KYSE450 PTX3-OV group.

In order to detect the expression of PTX3 in the tumor tissues of nude mice, we performed immunohistochemistry (IHC) staining. The

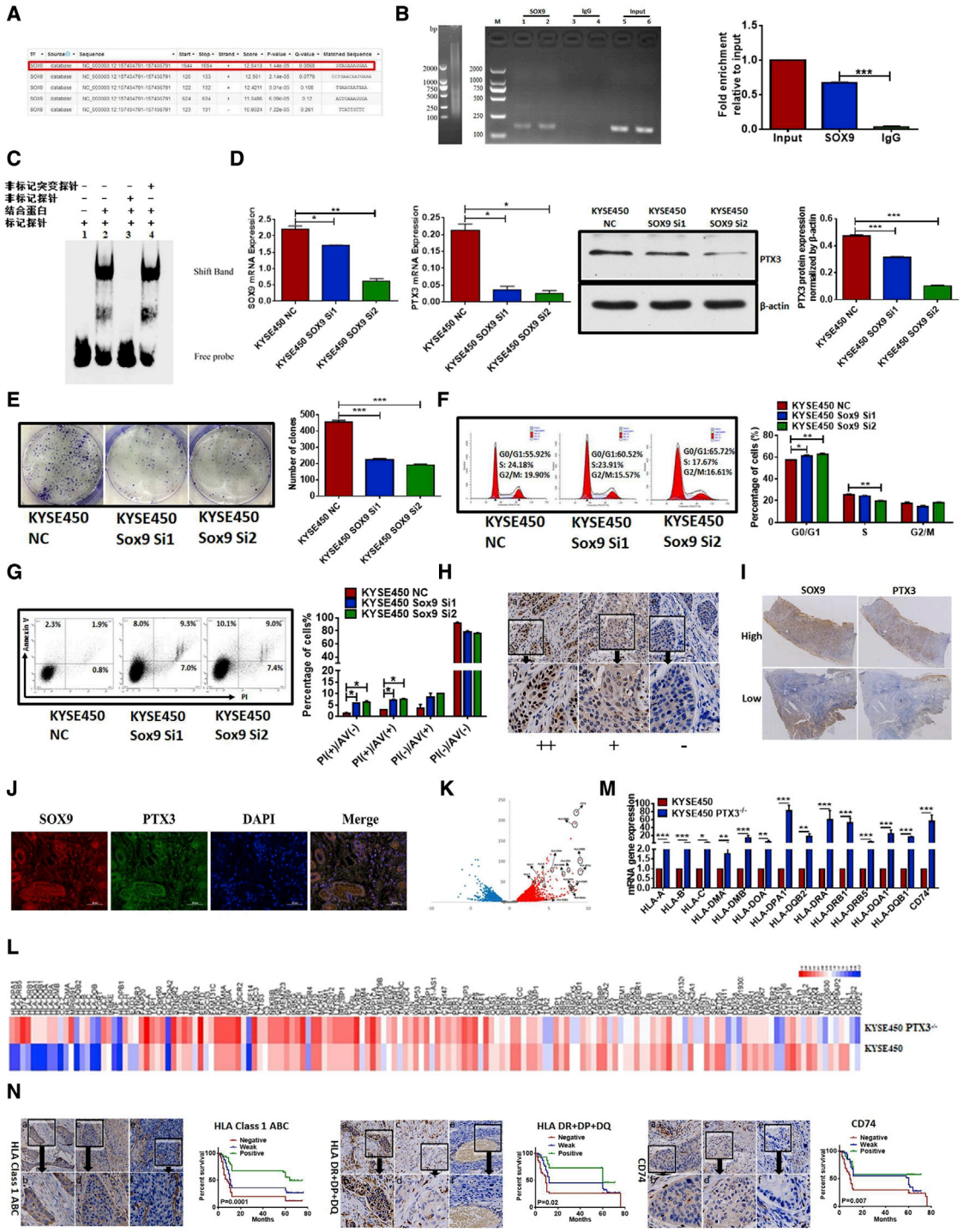

Figure 6. SOX9 regulates PTX3 expression and affects the HLA system

(A) Score of SOX9 binding sequence. (B) ChIP detects the combination of SOX9 and PTX3. Ultrasonic fragmentation of chromatin agarose gel electrophoresis, input chromatin immunoprecipitation experiment PCR analysis, and the relative binding rate obtained by comparing the gray value of input amplification product band scanning with 1 are shown. (C) EMSA verifies the binding of SOX9 and PTX3 *in vitro* (1, negative control; 2, experimental group; 3, cold competition; 4, mutation competition). (D) PTX3 expression is down-regulated after SOX9 silence. RT-PCR detects the transfection efficiency of SOX9 and the expression of PTX3 gene after SOX9 transfection, and western blot detects the expression of PTX3 protein after SOX9 transfection. (E) The effect of SOX9 silence on cell proliferation was detected by plate cloning experiment. (F) The effect of SOX9 silence on the cell cycle was detected by flow cytometry. (G) The effect of SOX9 silencing on cell apoptosis detected through flow cytometry is shown. (H) Expression

(legend continued on next page)

results are shown in Figure 7K. The KYSE450 group had the strongest PTX3 expression, and the KYSE450 administration group had a significant down-regulation of PTX3 expression. In the KYSE450 PTX3$^{-/-}$ group, only a small number of cells were weakly positive for PTX3, while in the KYSE450 PTX3$^{-/-}$ administration group, the expression of PTX3 was basically negative. The above results indicated that PTX3 is sensitive to docetaxel chemotherapy and may be a new potential therapeutic target. At the same time, we measured the expression of HLA-related proteins in tumor tissues of nude mice, and the results (Figure 7L) showed that the expressions of HLA class I ABC, HLA DR + DP + DQ, and CD74 in the KYSE450 PTX3$^{-/-}$ group were significantly higher than those in the KYSE450 group, which was consistent with the results of the 101 cases of human ESCC (Figure 6N).

DISCUSSION

Studies have reported that PTX3 can be produced by innate immune cells and plays an important role in innate immunity, regulation of inflammation, and matrix deposition through the interaction with several ligands.[7] PTX3 contributes to tumor-related inflammation, and its expression has been identified as a new diagnostic and prognostic biomarker for various types of cancer, including glioma,[11] prostate cancer,[12] lung cancer,[13] soft-tissue liposarcoma,[14] and pancreatic cancer.[15] Recent evidence reveals that the expression of PTX3 in tumors and adjacent liver tissues of patients with hepatocellular carcinoma is significantly up-regulated. PTX3 can accelerate the progression of hepatocellular carcinoma by activating epithelial-mesenchymal transition (EMT) and serves as a potential predictor and therapeutic target for hepatocellular carcinoma.[16] In addition, high PTX3 expression had been detected in the tissues of patients with small cell lung cancer, and it has been confirmed that elevated levels of PTX3 are associated with decrease in overall survival (OS) and recurrence-free survival (RFS). So PTX3 may be a useful prognostic marker and potential molecular target for treatment of patients with small cell lung cancer.[17] Considering the potential role of PTX3 in inflammation-related carcinogenesis, we explored the relationship between PTX3 and the occurrence and development of ESCC, in order to prove that PTX3 plays an important role in ESCC.

Cancer is a disorder of cell proliferation. In most cancers, every pathway that restricts the normal cell proliferation response of normal cells is disturbed. Apoptosis plays an important role in the development of multicellular organisms, and it directly affects the regulation and maintenance of cell populations under physiological and pathological conditions.[18] Imbalanced proliferation and inhibition of cell apoptosis are the core of all tumor development. Therefore, targeting cell proliferation, cycle, and apoptosis pathways has become an attractive intervention target for cancer treatment.[19,20] Our results indicated that PTX3 affected the proliferation, cycle, and apoptosis of KYSE450 cells and could be a new target for the treatment of ESCC.

Based on the research of the past few decades, the recent imbalance of cell energy has also been regarded as one of the signs of cancer.[21] Otto Warburg first proposed that tumor cells are different from normal cells, that is, even when oxygen is available, glycolysis is up-regulated and mitochondrial respiration is suppressed in tumor cells. This phenomenon is called the "Warburg effect." Several potential mechanisms of cellular energy disorders are related to mitochondrial dysfunction caused by mitochondrial DNA (mtDNA) mutations, mitochondrial enzyme defects, or oncogene and tumor suppressor changes.[22–24] Mitochondria are intracellular organelles in eukaryotic cells that participate in bioenergy metabolism and cell homeostasis, including the production of ATP through electron transfer and oxidative phosphorylation, the decomposition of fatty acids by the tricarboxylic acid (TCA) cycle oxidation metabolites and β-oxidation, the generation of ROS, and the initiation and execution of apoptosis.[25] Energy metabolism results showed that PTX3 affected cell energy metabolism, that is, after the PTX3 gene was knocked out, the cell's glycolytic capacity was impaired and inclined to oxidative phosphorylation.

SOX9 is up-regulated in many tumors and plays an important role as an oncogene in cancer progression.[21] In human transplantation models, the expression of SOX9 enhances the tumorigenic and metastasis-dissemination ability of breast cancer cells, and the conversion of EMT endows the cells with many characteristics that related to cancer stem cells.[26,27] A mouse model of basal cell carcinoma shows that SOX9 is a self-renewal-cell-like tumor stem cell, balancing the symmetrical and asymmetrical cell division during skin tumorigenesis.[28] Our research results showed that SOX9 is highly expressed in ESCC and is positively correlated with the expression of PTX3. Silencing SOX9 can inhibit cell proliferation, block cell cycle, and promote cell apoptosis.

The classic major histocompatibility complex (MHC) molecule is a highly polymorphic glycoprotein, which plays a central role in adaptive immunity through capturing and presenting peptide antigens of T cell receptor (TCR) expressed on T lymphocytes.[29] CD74, known as the constant chain of major MHC class II, is an important part of the

of SOX9 protein in ESCC is shown. a and b are positive for SOX9 protein expression in ESCC tissue (a, 200×; b, 400×); c and d are weakly positive for SOX9 protein expression in ESCC tissue (c, 200×; d, 400×); and e and f are negative expressions of SOX9 protein in ESCC tissue (e, 200×; f, 400×). The black arrow indicates the position of the 400× picture in the 200× picture. (I) IHC diagram of SOX9 and PTX3 in tissues of patients with ESCC is shown. (J) Immunofluorescence analysis of SOX9 and PTX3 expression in tissues of patients with ESCC is shown. (K) Gene volcano map of transcriptome sequencing differences is shown. Red represents up-regulation, blue represents down-regulation, and gray represents no difference. (L) All differential genes in the herpes simplex infection pathway are shown. (M) RT-PCR detects the expression of HLA-system-related genes. (N) Expression of HLA-system-related proteins HLA class I ABC, HLA DR + DP + DQ, and CD74 protein in ESCC tissues and the correlation between the expression of HLA-system-related proteins and the prognosis of patients with ESCC are shown. The black arrow indicates the position of the 400× picture in the 200× picture. *$p < 0.05$, **$p < 0.01$, and ***$p < 0.001$.

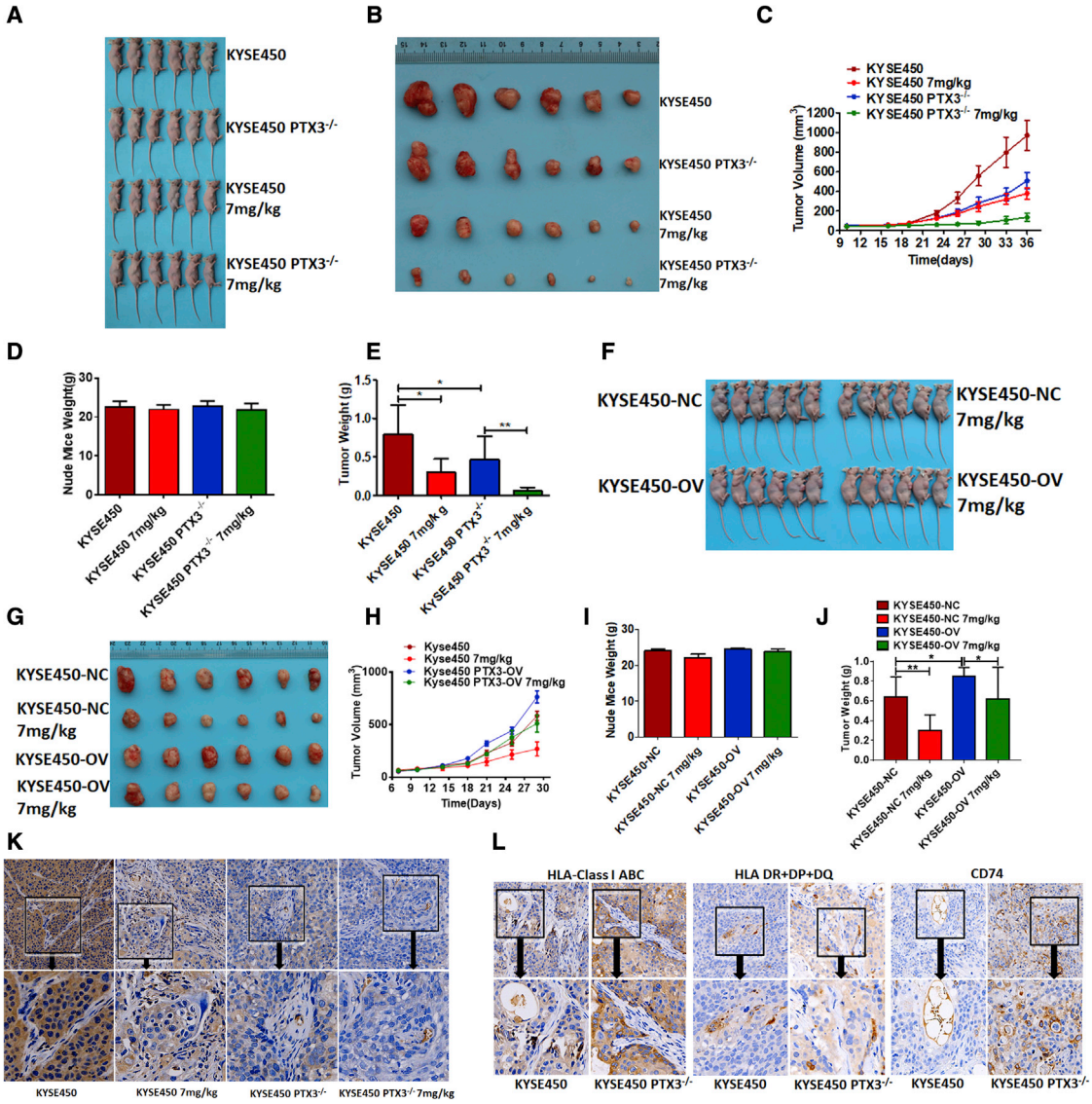

Figure 7. *In vitro* experiments to verify the effect of PTX3 on tumors

(A) 5×10^6 KYSE450 and KYSE450 PTX3$^{-/-}$ cells were injected subcutaneously into each nude mouse, and pictures of each group of mice after 4 weeks are shown. (B) Photographs of tumor tissues peeled off from mice in each group of (A) are shown. (C) KYSE450 and KYSE450 PTX3$^{-/-}$ tumor growth curves in each group are shown. (D) The body weights of mice in each group of KYSE450 and KYSE450 PTX3$^{-/-}$ are shown. (E) Histogram of the average tumor weights of mice in KYSE450 and KYSE450 PTX3$^{-/-}$ groups is shown. (F) 5×10^6 KYSE450-NC and KYSE450 PTX3-OV cells were injected subcutaneously into each nude mouse. Images of each mice group after 4 weeks are shown. (G) Photographs of tumor tissues stripped from mice in each group of (F) are shown. (H) Tumor growth curve of each group of KYSE450-NC and KYSE450 PTX3-OV is shown. (I) Body weights of mice in each group of KYSE450-NC and KYSE450 PTX3-OV are shown. (J) Histogram of the average tumor weight of mice in each group of KYSE450-NC and KYSE450 PTX3-OV is shown. (K) Expression of PTX3 in nude mouse tissues is shown. The black arrow indicates the position of the 400× picture in the 200× picture. (L) Expression of HLA-related proteins HLA class I ABC, HLA DR + DP + DQ, and CD74 in nude mouse tissues is shown.

functional expression of MHC class II restricted antigens and a key factor in anti-tumor immunity.[30] One of the hallmarks of cancer is that it can promote immune evasion by down-regulating HLA genes to reduce antigen presentation.[31] Reduced expression of HLA-I in tumors is an important immune escape mechanism for limiting the function of cytotoxic T cell (CTL) described in various types of cancers and is often associated with poor prognosis of patients and resistance to immunotherapy.[32] High-throughput transcriptome sequencing revealed that the HLA-system-related genes in KYSE450 PTX3$^{-/-}$ cells were significantly up-regulated. At the same time, in human ESCC tissues, the expression of HLA-system-related proteins was correlated with the survival time of patients. Patients with high expression of HLA-system-related proteins have a long survival period and favorable prognosis.

Table 3. The relationship between the expression of HLA-system-related proteins and the survival time of patients with ESCC

	Survival time			
Related proteins	n	≤1 year	≥5 years	p value[a]
HLA class I ABC				
Positive	37	12 (32.43%)	25 (67.57%)	
Weak positive	39	25 (64.10%)	14 (35.90%)	0.000
Negative	25	20 (80.00%)	5 (20.00%)	
HLA DR + DP + DQ				
Positive	15	4 (26.67%)	11 (73.33%)	
Weak positive	56	31 (55.36%)	25 (44.64%)	0.012
Negative	30	22 (73.33%)	8 (26.67%)	
CD74				
Positive	21	9 (42.86%)	12 (57.14%)	
Weak positive	33	15 (45.45%)	18 (54.55%)	0.033
Negative	47	33 (70.21%)	14 (29.79%)	

Nude mouse tumor formation experiments showed that knocking out the PTX3 can inhibit tumor formation *in vivo* and improve tumor-bearing mice's sensitivity to docetaxel. On the contrary, PTX3 overexpression model promoted the tumor formation *in vivo* and reduced tumor-bearing mice's sensitivity to docetaxel, which was consistent with the results of *in vitro* cell experiments. In tumor tissues of nude mice, the expression of HLA-system-related proteins in the PTX3 knockout group was higher than that in the control group, suggesting that PTX3 may affect the expression of HLA-system-related proteins. In conclusion, our study found that SOX9 gene can regulate the transcriptional expression of PTX3 directly, and the role of PTX3 in ESCC may be regulated by SOX9. We believe that external inflammatory stimuli regulate PTX3 through SOX9 transcription, which in turn affects the HLA system to promote tumor progression.

MATERIALS AND METHODS

Cell lines and cell culture

Esophageal epithelial cell line Het1A and ESCC cell lines KYSE140 and EC109 were obtained from the American Type Culture Collection (ATCC) in 2016, and the KYSE450 cell line was purchased from the German Collection of Microorganisms and Cultures (DSMZ) in 2015. Cells were routinely cultured in RPMI-1640 medium (Sigma, USA), supplemented with 10% fetal bovine serum (Gibco, USA), 100 U/mL of penicillin, and 100 μg/mL of streptomycin at 37°C in a 5% CO_2 humidified incubator.

RNA isolation and quantitative real-time PCR analysis

RNA was extracted from cells using TRIZOL reagent (TaKaRa, Japan). The Revert Aid First Strand cDNA Synthesis Kit (TaKaRa, Japan) was used for cDNA synthesis. The forward and reverse primer sequences are shown in Table 4. The quantitative real-time PCR using an SYBR Green PCR master mix (Qiagen, Germany) was performed with the AgilentMx3005P. The samples were amplified at 95°C for 5 min, 40 cycles of 95°C for10 s, and 60°C for 30 s. Relative gene expression was determined by normalizing the expression of each target gene to GAPDH. The data were analyzed by using $2^{-\Delta\Delta Ct}$.

Table 4. Primers for quantitative real-time PCR

Gene name	Sequence (5′-to-3′)
GAPDH	F: GCACTCTTCCAGCCTTCCTTCC
	R: TCACCTTCACCGTTCCAGTTTTT
PTX3	F: CTGGGAGACTCACAGGCTTC
	R: GACAAGACTCTGCTCCTCCG
HLA-A	F: TGGAGAGGAGCAGAGATACACC
	R: AGAACCAGGCCAGCAATGATG
HLA-B	F: TCATCTCAGTGGGCTACGTG
	R: GTGTGTTCCGGTCCCAATAC
HLA-C	F: GGTGGTGCCTTCTGGACAAG
	R: CTCTTCCTCCTACACATCATAGCG
HLA-DMA	F: CCTGCACACAGTGTACTGC
	R: CACCCGAGTGTTCTGGGAA
HLA-DMB	F: TGGCGAATGTCCTCTCACAG
	R: TGTGTGGCACAATTCTGAAGC
HLA-DOA	F: CCTACGGACCCGCCTTCTA
	R: GGCCTCGCTTTTCTTCAGG
HLA-DPA1	F: ATGCGCCCTGAAGACAGAATG
	R: ACACATGGTCCGCCTTGATG
HLA-DQB2	F: CAGATCAAAGTCCGGTGGTT
	R: TGGAAGGTCCAGTCACCATT
HLA-DRA	F: TCTGGCGGCTTGAAGAATTTG
	R: GGTGATCGGAGTATAGTTGGAGC
HLA-DRB1	F: CAGTTCCTCGGAGTGGAGAG
	R: CTCAGCATCTTGCTCTGTGC
HLA-DRB5	F: GCACAGAGCAAGATGCTGAG
	R: ACGAGTCCTGTTGGGTGAAG
HLA-DQA1	F: GGACCTGGAGAGGAAGGAGAC
	R: GTAGCAGCGGTAGAGTTGTAGC
HLA-DQB1	F: TTGATGCTGGCGATGCTGAG
	R: GCGTACTCCTCTCGGTTATAGATG
CD74	F: GATGACCAGCGCGACCTTATC
	R: GTGACTGTCAGTTTGTCCAGC

Protein isolation and western blot analysis

Cells were harvested and lysed with mixed radioimmunoprecipitation assay (RIPA) buffer containing 50 mM Tris-HCl (pH 7.5), 150 mM NaCl, 1% NP-40, 0.5% sodium deoxycholate, 0.1% SDS, and 1% PMSF (100×; CWBiotech, China) on ice for about 30 min and then centrifuged at 1,500 × *g* for 5 min at 4°C. Proteins were loaded to 12% SDS-PAGE and then transferred to PVDF (Millipore, USA) membrane. The membrane was blocked in Tris-buffered saline with Tween 20 (TBST) buffer containing 5% non-fat milk at room temperature (22°C) for 1 h and then probed with antibodies for PTX3

(Genetex, USA) and β-actin (Abcam, UK) at 4°C overnight, followed by incubating with respective horseradish-peroxidase-conjugated secondary antibody for 1 h at room temperature. Then, the membrane was exposed to a chemiluminescent reagent (enhanced chemiluminescence [ECL]) for about 5–10 min and exposed to X-ray photographic films in a darkroom, and the band densities were later quantified with ImageJ Software (NIH, USA).

Generation of PTX3 knockout and overexpressed cell lines

We constructed a model of PTX3 knockout in ESCC KYSE450 cell line by using CRISPR-Cas9 technology. Three gRNA sequences were designed for the target sequences of PTX3 in the first, second, and third exons, and they were respectively ligated to the lentiviral backbone plasmid. Then, they were transfected into 293T cells and their genomic DNAs were extracted. The target sequences were amplified by PCR and then digested to screen for the most efficient PTX3-gRNA.The virus was packaged with the most effective plasmid and infected KYSE450 cell line. After infection, the cells were screened with puromycin and the selected cells were cultured in single cells. Similarly, a lentiviral vector was used to establish the KYSE450 cell line model overexpression PTX3.

Cell proliferation assay

IncuCyte Imaging System was used for real-time assessment of cell proliferation for 4 days (Essen Biosciences, USA). The cells were cultured in 96-well plates (Corning, USA) at a density of 2,000 cells per well and incubated overnight in medium containing 10% fetal bovine serum (FBS). Then, we transferred the cells to IncuCyte apparatus, collected images (two/well) every 4 h, and used the corresponding software installed in the IncuCyte system to obtain the cell growth curves.

Cell cycle assay

Cells were collected by 0.05% trypsin without EDTA solution and fixed with ice-cold 75% ethanol at 4°C overnight. For cell cycle analysis, cells were stained with 2 μg/mL RNase A and 10 μg/mL PI. DNA contents were measured with BD LSRII flow cytometer and analyzed with Software FlowJo v.7.6.

Cell apoptosis assay

Cells were harvested and washed with ice-cold PBS and then resuspended in AV-binding buffer. Thereafter, PI (Sigma, USA) was added to the cell suspension and incubated for 15 min at room temperature in the dark. Following this, samples were immediately analyzed by flow cytometry (BD Biosciences, USA).

Migration assay

Migration assay was performed by wound healing test. The cells (3×10^4 cells/well) were dispensed into 96-well plates and incubated at 37°C, 5% CO2 overnight for wound healing test. Wounds were created by a 96-well scratcher with Incucyte ZOOM. Relevant parameters were set to take a picture every 6 h, and experiment results were analyzed after 24 h of culture. We seeded 5×10^4 cells in serum-free medium into the upper chamber, and 700 μL of medium containing 10% serum was added in lower chamber for transwell migration assay with a filter of transwell system (8.0 μm pore size, 24-well insert). After incubation of 24 h, cells were fixed with 4% paraformaldehyde, stained with 0.1% crystal violet, imaged, and counted under a microscope.

Chemotherapy sensitivity assay

Cells were seeded in a 96-well plate (2 × 103 cells/well), medicated medium was replaced after the cells adhere to the wall, and then we put them in the Incucyte ZOOM incubator. The relevant parameters were set to take pictures every 4 h. The medium was changed every 2 days. The experiment was completed after 5–7 days, and the results were analyzed.

Radiotherapy sensitivity assay

The cells were seeded in a 6-well plate (500 cells/well). After the cells were attached, the cells were irradiated with doses of 0 Gy, 2 Gy, 4 Gy, 6 Gy, and 8 Gy, respectively, according to the dose rate table, and three sub-wells were set for the same irradiation dose. After the irradiation, we replaced the medium with 3 mL fresh medium and continued to incubate. After 2 weeks, the cells were fixed with 4% paraformaldehyde and then stained with 0.1% crystal violet. Pictures were taken, and the number of clones in each well was counted.

Cellular energy metabolism assay

OCR and ECAR were measured using a Seahorse XF^{e}96 extracellular flux analyzer (Seahorse Bioscience, USA). Cells were seeded at a density of 5×10^4 cells/well in XF^{e}96 cell culture microplate (Seahorse Bioscience) and cultured overnight until they attached to the bottom. The cells were transferred into an assay medium supplemented with 1 mM pyruvate, 2 mM glutamine, and 10 mM glucose 1 h prior to the assay and incubated at 37°C. After baseline measurements, OCR was measured by adding FCCP and rotenone and antimycin A to each well, and ECAR was determined by adding oligomycin and 2-deoxy-D-glucose (2-DG).

ChIP assay

Cells were plated in a 10-cm culture dish, cultured for 24 h, and fixed with formaldehyde at a final concentration of 1%. After washing with PBS, the cells were resuspended in lysis buffer. The DNA was sheared into small fragments by sonication. After that, 100 μL of the sonicated product was added to 900 μL of Chip Dilution buffer and 20μL of 50× Protease Inhibitor Cocktail (PIC) and then incubated with Protein A + G agarose/Salmon Sperm DNA at 4°C for 2 h. The recovered supernatants were incubated with PTX3 antibody (Genetex, USA) or an isotype control IgG overnight. The immunoprecipitated DNA was retrieved from the beads by incubating with elution buffer (0.5 g SDS + 0.42 g $NaHCO_3$ + 50 mL water) at 65°C overnight and recovered with phenol chloroform extraction. To verify the success of the ChIP experiment, PCR experiment was performed using primers designed to predict binding sites (Table 5). The template was the input, the target antibody immunoprecipitated DNA, and negative antibody (IgG) immunoprecipitated DNA.

Table 5. Primers for quantitative real-time PCR

Gene name	Sequence (5′-to-3′)
PTX3-F	CCTATGTCCATTTGGTAGTTGTCC
PTX3-R	AGCTCAAGGCATGGATTAAGTG

EMSA

Nuclear protein and cytoplasmic protein were extracted according to the manufacturer's instructions (Beyotime, China). EMSA was performed with the LightShift Chemiluminescent EMSA Kit (Thermo Fisher Scientific, USA) following the manufacturer's instructions. DNA binding reactions were performed in 20-μL samples (Table 6). The samples were run on 5.5% non-denaturing polyacrylamide gels with 0.5× Tris, borate, and EDTA (TBE) buffer and transferred to a nylon membrane. The membranes were scanned using Alpha Innotech (Alpha, USA).

Transient transfection

The siRNA was transfected with Lipofectamine 3000 at a final concentration of 20 nM according to the instructions and divided into a control group and an experimental group. The siRNA sequence of SOX9 is as follows: SOX9 siRNA-1 (target sequence: 5′-AACUCC AGCUCCUACUACAGCTT-3′), SOX9 siRNA-2 (target sequence: 5′-GCAGCGACGUCAUCUCCAAUU-3′), and control siRNA (target sequence: 5′-UUCUCCGAACGUGUCACGUTT-3′). After transfection for 48 h, cells were harvested for subsequent experimental studies.

Immunofluorescence detection of SOX9 and PTX3 co-expression

ESCC tissues were stained with SOX9 and PTX3 antibodies, respectively. Cy3- and fluorescein isothiocyanate (FITC)-conjugated secondary antibodies were used to detect primary antibodies. The stained cells were counterstained with DAPI and photographed using an inverted fluorescence microscope.

Transcriptomic analysis

Samples were sequenced at BGI (Shenzhen, Guangdong, China) using transcriptome sequencing technology, with three replicates per group. The methods of transcriptomic analysis were described in our previous study.[33]

Xenograft model in nude mice

Four-week-old specific-pathogen-free (SPF) male nude mice (Beijing Vital River Laboratory Animal Technology, China) weighing 19 ± 2 g were divided randomly into eight groups (six mice/group). Subcutaneously transplanted nude mice models were established, and their drug sensitivity to docetaxel was observed. Each group received hypodermic injections of either scrambled KYSE450, KYSE450 PTX3$^{-/-}$, KYSE450-NC, or KYSE450 PTX3-OV cells (5×10^6 cells in 100 μL PBS). Mice were weighed every 3 days, and tumor size was measured. Tumor volume was obtained by the following formula: (length × width^2)/2. Mice were sacrificed by cervical dislocation on the 31st day after cell implantation. The tumors were collected for IHC analysis.

Table 6. Protein and probe reaction

Reagent	Negative control	Sample group	Competition group
10× binding buffer	2	2	2
1 μg/μL poly (dI.dC)	1	1	1
50% glycerol	1	1	1
1% NP-40	1	1	1
100 mM Mgcl	1	1	1
200 mM EDTA	1	1	1
Protein	−	+	+
Labeled probe (200 fmol)	+	+	+
Unlabeled probe (40 pmol)	−	−	+
H_2O	+	+	+
Total volume	20 μL	20 μL	20 μL

Patients and samples

In this study, 294 cases of formalin-fixed and paraffin-embedded ESCC specimens were included. All the patients were diagnosed and surgically treated in AnYang Tumor Hospital between 2005 and 2017. Any patients treated with chemotherapy, hormone therapy, or radiotherapy before surgery were excluded from the study. Written informed consent was obtained from all the patients. The whole consent procedure was in compliance with the ethical standards defined by Institutional Ethics Review Committee of The First Affiliated Hospital of Zhengzhou University.

IHC

The methods of IHC analysis were described in our previous study. Protein expression was assessed by the percentage of positive stained-tumor cells and the intensity of staining. The percentage scoring of immunoreactive tumor cells was as follows: 0 (0%), 1 (<25%), 2 (25%–50%), and 3 (>50%). The staining intensities were scored visually and stratified as follows: 0 (negative), 1 (light brown), 2 (brown), and 3 (dark brown). A final immunoreactivity score was obtained for each case by adding the percentage and the intensity score. For statistical analysis of ESCC tissue samples, 0 was negatively expressed, 1–4 was weakly positive, and 5 to 6 was positive.

Statistical analysis

Statistical analysis was performed using SPSS 19.0 statistical software or GraphPad prism 5.0. Results are shown as mean ± standard deviation (SD). Independent-sample or paired t test was performed to analyze the differences between two groups with normally distributed continuous variables. Chi-square test was performed to quantify the IHC correlation of patient-derived samples. Survival curves were performed by the Kaplan-Meier method, and groups were compared using log rank tests. In all cases, a two-tailed $p < 0.05$ was considered statistically significant; *$p < 0.05$, **$p < 0.01$, and ***$p < 0.001$.

SUPPLEMENTAL INFORMATION

Supplemental information can be found online at https://doi.org/10.1016/j.omto.2022.02.005.

ACKNOWLEDGMENTS

This study was supported by the National Natural Science Foundation of China (Grant No. 82104608, 82002433) Henan Province Medical Science and Technology Research Plan Joint Construction Project (LHGJ20190055, LHGJ20190003), Special Project of Traditional Chinese Medicine Research in Henan Province (Grant No. 20-21ZY2311), Young and Middle-aged Health Science and Technology Innovation Talents in 2020 (Grant No. YXKC2020049).

AUTHOR CONTRIBUTIONS

L.L. and Z.S. designed and coordinated the research. Z.F. and X.L. mainly completed and drafted the manuscript. Y.Z., J.S., and H.W. helped with the research and analyzed the data. X.D., Y.B., and K.F. provided substantial contributions to conception of the manuscript and participated in drafting.

DECLARATION OF INTERESTS

The authors declare no competing interests.

REFERENCES

1. Bray, F., Ferlay, J., Soerjomataram, I., Siegel, R.L., Torre, L.A., and Jemal, A. (2018). Global cancer statistics 2018: GLOBOCAN estimates of incidence and mortality worldwide for 36 cancers in 185 countries. CA Cancer J. Clin. *68*, 394–424.
2. Wu, X., Lim, Z.F., Li, Z., Gu, L., Ma, W., Zhou, Q., Su, H., Wang, X., Yang, X., and Zhang, Z. (2017). NORAD expression is associated with adverse prognosis in esophageal squamous cell carcinoma. Oncol. Res. Treat *40*, 370–374.
3. Balkwill, F., and Mantovani, A. (2001). Inflammation and cancer: back to Virchow? Lancet *357*, 539–545.
4. Mantovani, A., Allavena, P., Sica, A., and Balkwill, F. (2008). Cancer-related inflammation. Nature *454*, 436–444.
5. Moss, S.F., and Blaser, M.J. (2005). Mechanisms of disease: inflammation and the origins of cancer. Nat. Clin. Pract. Oncol. *2*, 90–97, quiz 91 p following 113.
6. Breviario, F., d'Aniello, E.M., Golay, J., Peri, G., Bottazzi, B., Bairoch, A., Saccone, S., Marzella, R., Predazzi, V., Rocchi, M., et al. (1992). Interleukin-1-inducible genes in endothelial cells. cloning of a new gene related to C-reactive protein and serum amyloid P component. J. Biol. Chem. *267*, 22190–22197.
7. Inforzato, A., Doni, A., Barajon, I., Leone, R., Garlanda, C., Bottazzi, B., and Mantovani, A. (2013). PTX3 as a paradigm for the interaction of pentraxins with the complement system. Semin. Immunol. *25*, 79–85.
8. Garlanda, C., Bottazzi, B., Bastone, A., and Mantovani, A. (2005). Pentraxins at the crossroads between innate immunity, inflammation, matrix deposition, and female fertility. Annu. Rev. Immunol. *23*, 337–366.
9. Bonavita, E., Gentile, S., Rubino, M., Maina, V., Papait, R., Kunderfranco, P., Greco, C., Feruglio, F., Molgora, M., Laface, I., et al. (2015). PTX3 is an extrinsic oncosuppressor regulating complement-dependent inflammation in cancer. Cell *160*, 700–714.
10. Bottazzi, B., Inforzato, A., Messa, M., Barbagallo, M., Magrini, E., Garlanda, C., and Mantovani, A. (2016). The pentraxins PTX3 and SAP in innate immunity, regulation of inflammation and tissue remodelling. J. Hepatol. *64*, 1416–1427.
11. Fan, Z., Li, L., Li, X., Zhang, M., Dou, M., Zhao, J., Cao, J., Deng, X., Zhang, M., Li, H., et al. (2019). Anti-senescence role of heterozygous fumarate hydratase gene knockout in rat lung fibroblasts *in vitro*. Aging *11*, 573–589.
12. Locatelli, M., Ferrero, S., Martinelli Boneschi, F., Boiocchi, L., Zavanone, M., Maria Gaini, S., Bello, L., Valentino, S., Barbati, E., Nebuloni, M., et al. (2013). The long pentraxin PTX3 as a correlate of cancer-related inflammation and prognosis of malignancy in gliomas. J. Neuroimmunol. *260*, 99–106.
13. Stallone, G., Cormio, L., Netti, G.S., Infante, B., Selvaggio, O., Fino, G.D., Ranieri, E., Bruno, F., Prattichizzo, C., Sanguedolce, F., et al. (2014). Pentraxin 3: a novel biomarker for predicting progression from prostatic inflammation to prostate cancer. Cancer Res. *74*, 4230–4238.
14. Diamandis, E.P., Goodglick, L., Planque, C., and Thornquist, M.D. (2011). Pentraxin-3 is a novel biomarker of lung carcinoma. Clin. Cancer Res. *17*, 2395–2399.
15. Willeke, F., Assad, A., Findeisen, P., Schromm, E., Grobholz, R., von Gerstenbergk, B., Mantovani, A., Peri, S., Friess, H.H., Post, S., et al. (2006). Overexpression of a member of the pentraxin family (PTX3) in human soft tissue liposarcoma. Eur. J. Cancer *42*, 2639–2646.
16. Kondo, S., Ueno, H., Hosoi, H., Hashimoto, J., Morizane, C., Koizumi, F., Tamura, K., and Okusaka, T. (2013). Clinical impact of pentraxin family expression on prognosis of pancreatic carcinoma. Br. J. Cancer *109*, 739–746.
17. Song, T., Wang, C., Guo, C., Liu, Q., and Zheng, X. (2018). Pentraxin 3 overexpression accelerated tumor metastasis and indicated poor prognosis in hepatocellular carcinoma via driving epithelial-mesenchymal transition. J. Cancer *9*, 2650–2658.
18. Liu, C., Yao, Y., and Wang, W. (2014). Pentraxin-3 as a prognostic marker in patients with small-cell lung cancer. Med. Oncol. *31*, 207.
19. Leist, M., and Jaattela, M. (2001). Four deaths and a funeral: from caspases to alternative mechanisms. Nat. Rev. Mol. Cell Biol. *2*, 589–598.
20. Evan, G.I., and Vousden, K.H. (2001). Proliferation, cell cycle and apoptosis in cancer. Nature *411*, 342–348.
21. Senderowicz, A.M. (2004). Targeting cell cycle and apoptosis for the treatment of human malignancies. Curr. Opin. Cell Biol. *16*, 670–678.
22. Hanahan, D., and Weinberg, R.A. (2011). Hallmarks of cancer: the next generation. Cell *144*, 646–674.
23. Cairns, R.A., Harris, I.S., and Mak, T.W. (2011). Regulation of cancer cell metabolism. Nat. Rev. Cancer *11*, 85–95.
24. Wallace, D.C. (2012). Mitochondria and cancer. Nat. Rev. Cancer *12*, 685–698.
25. Upadhyay, M., Samal, J., Kandpal, M., Singh, O.V., and Vivekanandan, P. (2013). The Warburg effect: insights from the past decade. Pharmacol. Ther. *137*, 318–330.
26. Galluzzi, L., Kepp, O., and Kroemer, G. (2012). Mitochondria: master regulators of danger signalling. Nat. Rev. Mol. Cell Biol. *13*, 780–788.
27. Guo, W., Keckesova, Z., Donaher, J.L., Shibue, T., Tischler, V., Reinhardt, F., Itzkovitz, S., Noske, A., Zurrer-Hardi, U., Bell, G., et al. (2012). Slug and Sox9 cooperatively determine the mammary stem cell state. Cell *148*, 1015–1028.
28. Mani, S.A., Guo, W., Liao, M.J., Eaton, E.N., Ayyanan, A., Zhou, A.Y., Brooks, M., Reinhard, F., Zhang, C.C., Shipitsin, M., et al. (2008). The epithelial-mesenchymal transition generates cells with properties of stem cells. Cell *133*, 704–715.
29. Larsimont, J.C., Youssef, K.K., Sanchez-Danes, A., Sukumaran, V., Defrance, M., Delatte, B., Liagre, M., Baatsen, P., Marine, J.C., Lippens, S., et al. (2015). Sox9 controls self-renewal of oncogene targeted cells and links tumor initiation and invasion. Cell Stem Cell *17*, 60–73.
30. Rudolph, M.G., Stanfield, R.L., and Wilson, I.A. (2006). How TCRs bind MHCs, peptides, and coreceptors. Annu. Rev. Immunol. *24*, 419–466.
31. Accolla, R.S., Lombardo, L., Abdallah, R., Raval, G., Forlani, G., and Tosi, G. (2014). Boosting the MHC class II-restricted tumor antigen presentation to CD4+ T helper cells: a critical issue for triggering protective immunity and Re-orienting the tumor microenvironment toward an anti-tumor state. Front Oncol. *4*, 32.
32. McGranahan, N., Rosenthal, R., Hiley, C.T., Rowan, A.J., Watkins, T.B.K., Wilson, G.A., Birkbak, N.J., Veeriah, S., Van Loo, P., Herrero, J., et al. (2017). Allele-specific HLA loss and immune escape in lung cancer evolution. Cell *171*, 1259–1271.e11.
33. Seliger, B., Stoehr, R., Handke, D., Mueller, A., Ferrone, S., Wullich, B., Tannapfel, A., Hofstaedter, F., and Hartmann, A. (2010). Association of HLA class I antigen abnormalities with disease progression and early recurrence in prostate cancer. Cancer Immunol. Immunother. *59*, 529–540.